International Journal of Applied Mechanics
Vol. 7, No. 4 (2015) 1550053 (29 pages)

DOI: 10.1142/S1758825115500532

Imperial College Press
www.icpress.co.uk

Vibration and Acoustic Responses of an Orthotropic Composite Conical Shell in a Hygroscopic Environment

Xin Zhao and Yueming Li*

State Key Laboratory for Strength and Vibration of Mechanical Structures
Xi'an Jiaotong University, Xi'an 710049, P. R. China
**liyueming@mail.xjtu.edu.cn*

Received 30 October 2014
Revised 8 May 2015
Accepted 21 June 2015
Published 20 August 2015

The vibration and acoustic radiation for an orthotropic composite conical shell in a hygroscopic environment are explored through the wave propagation approach and Galerkin method. Theoretical results of the natural vibration and far field sound pressure are presented with incremental moisture content. The effects of incremental stiffness and different semi-vertex angle on the acoustic radiation characteristics are studied too. It is found that the natural frequencies decrease with incremental moisture content. The wavenumbers associated with the lowest frequency mode reaches the modal indices corresponding to the lowest buckling mode near the critical buckling moisture content. With the increasing moisture content, a shifting of natural frequencies toward lower frequency band could be observed in lower frequency band of the modal density in constant frequency band. The overall sound pressure level (SPL) decreases generally with the moisture content, but shows a marginal increase near the critical buckling moisture content. The modal density and overall SPL decrease with the incremental stiffness generally, which increases with the decrease of the semi-vertex angle.

Keywords: Vibration; acoustic radiation; orthotropic conical shell; hygroscopic environment.

1. Introduction

The thin orthotropic composite conical shells have many applications in the aerospace industry such as aircraft, missile and launcher. It is very important to investigate the vibration and acoustic radiation from conical shells in order to design new aircrafts. The composite conical shells are typically exposed to moist environment in the service, especially in long-term storage period. The matrix in an orthotropic composite conical shell is more susceptible to the hygroscopic condition than the fiber, and the hygroscopic strains and stresses are not equal in the

*Corresponding author.

meridianal and circumferential axes due to the different moisture expansion coefficients. Hygroscopic stresses due to the moisture absorbed during the long-term storage period may induce buckling and dynamic instability in structures, and the pre-stress effect of hygroscopic load will affect the dynamic behavior of the conical shell and then cause the changes of acoustic radiation characteristics.

Some researchers studied buckling and free vibration behavior of composite cylindrical shells/shell panels due to hygroscopic load. Shen [2001] investigated the effect of hygroscopic conditions on the buckling and post-buckling of shear deformable laminated cylindrical shells subjected to combined loading of axial compression and external pressure. The results showed that the hygroscopic environment had a significant effect on the interactive buckling load as well as post-buckling response of the shell. Parhi *et al.* [2001] investigated the free vibration and transient response analysis of multiple delaminated doubly curved composite shells subjected to a hygroscopic environment by a quadratic isoparametric finite element formulation based on the first-order shear deformation theory. The results showed that the degradation in the natural frequencies and the increase in the amplitude of dynamic displacements and stresses are influenced by the degree of moisture concentration.

A few researchers carried out the studies on the thermal buckling, free vibration or acoustic radiation of conical shell. Naj *et al.* [2008] studied thermal and mechanical instability of truncated conical shell made of functionally graded material. The equilibrium and stability equations for simply supported functionally graded conical shells were obtained. Torabi *et al.* [2013] analyzed functionally graded conical shell integrated with piezoelectric layers that was subjected to combined action of thermal and electrical loads. The prebuckling forces were obtained considering the membrane solutions of linear equilibrium equations. Tong [1993] explored the free vibration of orthotropic conical shell. The displacements of conical shell are described by the power series. Lam and Li [1999a, 1999b] investigated the free vibration of a rotating truncated circular isotropic and orthotropic conical shell by Galerkin method. Caresta and Kessissoglou [2008] used power series to solve the dynamic response of fluid loading conical shell. Fluid loadings are taken into account by dividing the conical shell into narrow strips, which are considered to be cylindrical shell. The displacements of conical shell must be described by many segment cones in their study. Luo and Schmidt [2009] developed a model of three-dimensional propagation and scattering around a seamount for an offset acoustic source. The conical seamount is approximated by a number of independent ring-shaped sectors. Cao *et al.* [2011] investigated acoustic radiation from cross-plied laminated conical shells and explored a theoretical model of acoustic radiation from conical shells. The far field sound pressure is found in the wavenumber domain by the superposition of acoustic radiation from the small cylinder segments divided by the conical shell.

Wave propagation approach has been used to study the vibration and sound radiation characteristic of cylindrical shells by several researchers. Zhang *et al.* [2001]

and Zhang [2002] analyzed the coupled structural-acoustic of cylindrical shells using the wave propagation method and with the method the calculation of coupled frequency of submerged cylindrical shells was relatively easy, quick but with good accuracy. The wave propagation approach was used by Gan *et al.* [2009] to analyze the free vibration of ring-stiffened cylindrical shell under initial hydrostatic pressure. It proved that the wave propagation approach is accurate for calculation of frequency of ring-stiffened cylindrical shell for shear diaphragm–shear diaphragm boundary conditions. Cao *et al.* [2012] studied the sound radiation from shear deformable stiffened laminated cylindrical shells in terms of sound pressure and the helical wave spectra. The far field sound pressure was derived by using the Fourier wavenumber transform and stationary phase method.

Some researchers have focused the wave propagation in heterogeneous materials. They found that the wave exhibits strong interaction within microstructures when wavelength is approaching the microstructural size, and the interaction will significantly alter the transient dynamic solution of wave propagation in the structure. In some case, the wave may stop propagating which is named as "acoustic bandgaps" or "phononic bandgaps". Kafesaki *et al.* [1995] presented band structure results for elastic waves in periodic composite materials consisting of scatterers embedded in a homogeneous polymer matrix. The wide full bandgaps are found in fCC, bCC and SC structures for a wide range of filling ratios. Suzuki and Yu [1998] developed a computational method based on the plane wave expansion to study elastic waves in periodic elastic media. The existence of elastic wave bandgaps was demonstrated theoretically in the face centered cubic lattice structures based on polyethylene background with spherical isotropic tungsten scatterers. Based on Mindlin's microelastic continuum theory, Gonella *et al.* [2011] introduced a wave propagation simulation methodology as a tool to dynamically characterize microstructured solids in a way that naturally accounts for their inherent heterogeneities. Hui and Oskay [2014] developed a new high order computational homogenization model that capture the dispersion and micro-inertia effects in composites and other heterogeneous media subjected to dynamic loading conditions.

Vibration and acoustic radiation of plates and shells in thermal or hygroscopic environment are rather, in comparison, limited in the literature. Lyrintzis and Bofilios [1990] presented an analytical study to predict dynamic response and noise transmission of discretely stiffened multi-layered composite panels and examined the effects of the temperature and high humidity. The results indicate that thermal and moisture effects are very important in predicting deflections and transmitted noise. Jeyaraj *et al.* [2011] adopted commercial finite element software to study the vibration and acoustic response characteristics of an isotropic cylindrical shell with clamped boundary conditions under a thermal environment. They found that there is a significant change in the vibration mode shapes and ring frequency toward the lowest natural frequency with an increase in temperature. Geng and Li [2012] studied the vibration and acoustic radiation characteristics of a thermally stressed

plate theoretically. They found that the natural frequencies of the plate reduce with temperature rise and the response curves float to lower frequency range. Zhao *et al.* [2013] investigated the vibration and acoustic response characteristics of an orthotropic laminated composite plate in a hygroscopic environment theoretically. The initial hygroscopic stress and mass addition caused by material moisture absorption are considered in the governing equations of orthotropic plate. They found the dynamic response and sound radiation float to lower frequencies with elevated moisture content and the coincidence frequency decreases with the enhanced stiffness.

The studies on vibration and sound radiation characteristics for the orthotropic conical shell under the hygroscopic environment are very few. In this work, the vibration and acoustic responses of an orthotropic truncated circular composite conical shell under hygroscopic environment are explored through the wave propagation approach and Galerkin method. The effects of hygroscopic stress and mass addition caused by moisture absorption are considered in the governing equations. To examine the validity of the present solution, comparisons are made against the frequency parameters with the previous work for an isotropic conical shell. The natural frequency characteristic and far field sound pressure of orthotropic conical shell with incremental moisture content are analyzed. The influences of enhanced stiffness by decreasing the ratio of circumferential modulus to the meridianal of the conical shell on the acoustic responses characteristics are studied, and the effects of different semi-vertex angle of conical shell on the acoustic responses are discussed too. Since the method adopted in this paper is based on harmonic forcing response and does not include local wave interaction within microstructures, therefore it is not able to deal with short wave propagation problems.

2. Formulation

The geometry and co-ordinate system of a truncated orthotropic circular conical shell is shown in Fig. 1, where α is the semi-vertex angle, h is the thickness, L_1 and

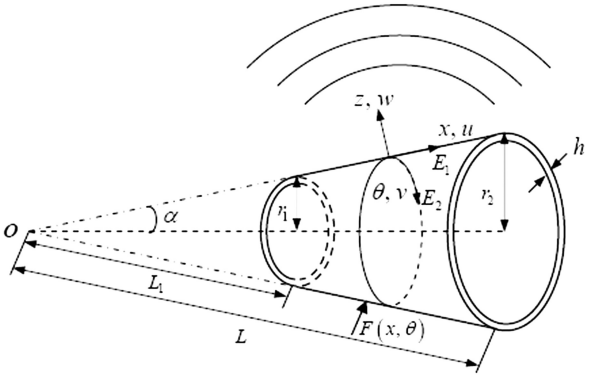

Fig. 1. Orthotropic conical shell and coordinate system.

L are the length of the small end and large end in the meridianal direction, respectively, r_1 and r_2 are the radii at the two ends. The curvilinear coordinate system is defined as $(x,\ \theta,\ z)$, where x and θ coincide with meridianal and circumferential directions, respectively, and z is perpendicular to the $x-\theta$ plane and its direction is inwards normal of the conical shell, and u, v, w are the displacements of the middle surface of conical shell. E_1 and E_2 are the meridianal and circumferential elasticity modulus in the principal material directions, respectively. The conical shell is composed of N layer laminas, and all laminas are orthotropic and the material principal directions are coincident with the coordinate system, so the composite conical shell bonding together with the lamina having the same principal coordinate system can be assumed an orthotropic composite conical shell. The conical shell is excited by harmonic point force $F(x,\theta)$.

2.1. *In-plane force induced by hygroscopic stress*

The normal and shear strains at a point with distance z from the middle surface of the conical shell according to the Love–Kirchhoff assumptions are [Brush and Almroth, 1975]:

$$\begin{aligned}\varepsilon_x &= \varepsilon_{xm} + zk_x,\\ \varepsilon_\theta &= \varepsilon_{\theta m} + zk_\theta,\\ \gamma_{x\theta} &= \gamma_{x\theta m} + zk_{x\theta},\end{aligned} \tag{1}$$

where ε_{xm} and $\varepsilon_{\theta m}$ are the mid-plane normal strains, $\gamma_{x\theta m}$ is the mid-plane shear strain, k_x and k_θ are the mid-plane curvature changes and $k_{x\theta}$ is mid-plane twist change. The linear strain–displacement relations, the strains, curvature, and twist changes of the mid-plane are:

$$\begin{aligned}\varepsilon_{xm} &= \frac{\partial u}{\partial x},\\ \varepsilon_{\theta m} &= \frac{1}{x\sin\alpha}\frac{\partial v}{\partial\theta} + \frac{u}{x} + \frac{w}{x\tan\alpha},\\ \gamma_{x\theta m} &= \frac{1}{x\sin\alpha}\left(x\sin\alpha\frac{\partial v}{\partial x} + \frac{\partial u}{\partial\theta} - v\sin\alpha\right),\\ k_x &= -\frac{\partial^2 w}{\partial x^2},\\ k_\theta &= \frac{1}{x^2\sin^2\alpha}\left(-\frac{\partial^2 w}{\partial\theta^2} + \cos\alpha\frac{\partial v}{\partial\theta} - x\sin^2\alpha\frac{\partial w}{\partial x}\right),\\ k_{x\theta} &= \frac{2}{x^2\sin\alpha}\left(\frac{\partial w}{\partial\theta} - x\frac{\partial^2 w}{\partial x\partial\theta} - v\cos\alpha + x\cos\alpha\frac{\partial v}{\partial x}\right).\end{aligned} \tag{2}$$

Based on the linear constitutive law in plane stress conditions, for the thin orthotropic conical stresses are functions of strains and moisture content as [Kaw,

2006; Whitney and Ashton, 1971]:

$$\begin{aligned}
\sigma_x &= \frac{E_1}{1-\mu_{12}\mu_{21}}(\varepsilon_{xm}+\mu_{21}\varepsilon_{\theta m}+zk_x+\mu_{21}zk_\theta)-\frac{E_1(\beta_1+\mu_{21}\beta_2)\Delta C}{1-\mu_{12}\mu_{21}},\\
\sigma_\theta &= \frac{E_2}{1-\mu_{12}\mu_{21}}(\varepsilon_{\theta m}+\mu_{12}\varepsilon_{xm}+zk_\theta+\mu_{12}zk_x)-\frac{E_2(\beta_2+\mu_{12}\beta_1)\Delta C}{1-\mu_{12}\mu_{21}},\\
\sigma_{x\theta} &= G_{12}(\gamma_{x\theta m}+zk_{x\theta}),
\end{aligned} \tag{3}$$

where β_1 and β_2 are the meridianal and circumferential coefficients of hygroscopic expansion in the principal material directions, respectively. μ_{12} and μ_{21} are the Poisson's ratios. $\Delta C(\%) = C_f - C_i$ is denoted as the moisture content change, and $C_i(\%)$ and $C_f(\%)$ are the initial and final uniform moisture content of the orthotropic conical shell.

Considering that based on the thin shell theory, the force and moment resultants are:

$$\begin{aligned}
N_x &= \int_{-h/2}^{h/2}\sigma_x dz, \quad N_\theta = \int_{-h/2}^{h/2}\sigma_\theta dz, \quad N_{x\theta} = \int_{-h/2}^{h/2}\sigma_{x\theta} dz,\\
M_x &= \int_{-h/2}^{h/2}\sigma_x z dz, \quad M_\theta = \int_{-h/2}^{h/2}\sigma_\theta z dz, \quad M_{x\theta} = \int_{-h/2}^{h/2}\sigma_{x\theta} z dz.
\end{aligned} \tag{4}$$

Substituting Eqs. (3) into Eqs. (4) yields:

$$\begin{aligned}
N_x &= \int_{-h/2}^{h/2}\left[\frac{E_1}{1-\mu_{12}\mu_{21}}(\varepsilon_{xm}+\mu_{21}\varepsilon_{\theta m}+zk_x+\mu_{21}zk_\theta)-\frac{E_1(\beta_1+\mu_{21}\beta_2)\Delta C}{1-\mu_{12}\mu_{21}}\right]dz\\
&= K_{11}\varepsilon_{xm}+K_{12}\varepsilon_{\theta m}-\frac{E_1 h(\beta_1+\nu_{21}\beta_2)\Delta C}{1-\mu_{12}\mu_{21}} = K_{11}\varepsilon_{xm}+K_{12}\varepsilon_{\theta m}-N_x^C,\\
N_\theta &= \int_{-h/2}^{h/2}\left[\frac{E_2}{1-\mu_{12}\mu_{21}}(\varepsilon_{\theta m}+\mu_{12}\varepsilon_{xm}+zk_\theta+\mu_{12}zk_x)-\frac{E_2(\beta_2+\mu_{12}\beta_1)\Delta C}{1-\mu_{12}\mu_{21}}\right]dz\\
&= K_{21}\varepsilon_{xm}+K_{22}\varepsilon_{\theta m}-\frac{E_2 h(\beta_2+\mu_{12}\beta_1)\Delta C}{1-\mu_{12}\mu_{21}} = K_{21}\varepsilon_{xm}+K_{22}\varepsilon_{\theta m}-N_\theta^C,\\
N_{x\theta} &= \int_{-h/2}^{h/2}G_{12}(\gamma_{x\theta m}+zk_{x\theta})dz = K_{66}\gamma_{x\theta m},\\
M_x &= \int_{-h/2}^{h/2}\left[\frac{E_1}{1-\mu_{12}\mu_{21}}(\varepsilon_{xm}+\mu_{21}\varepsilon_{\theta m}+zk_x+\mu_{21}zk_\theta)\right.\\
&\quad\left.-\frac{E_1(\beta_1+\mu_{21}\beta_2)\Delta C}{1-\mu_{12}\mu_{21}}\right]zdz\\
&= D_{11}k_x+D_{12}k_\theta,
\end{aligned}$$

$$
\begin{aligned}
M_\theta &= \int_{-h/2}^{h/2} \left[\frac{E_2}{1-\mu_{12}\mu_{21}} (\varepsilon_{\theta m} + \mu_{12}\varepsilon_{xm} + zk_\theta + \mu_{12} zk_x) \right. \\
&\quad \left. - \frac{E_2(\beta_2 + \mu_{12}\beta_1)\Delta C}{1-\mu_{12}\mu_{21}} \right] z dz \\
&= D_{21}k_x + D_{22}k_\theta, \\
M_{x\theta} &= \int_{-h/2}^{h/2} G_{12}(\gamma_{x\theta m} + zk_{x\theta}) z dz = D_{66}k_{x\theta},
\end{aligned} \tag{5}
$$

where K_{ij} and $D_{ij} (i, j = 1, 2, 6)$ are the film stiffness and bending stiffness as given below:

$$
\begin{aligned}
K_{11} &= \frac{E_1 h}{(1-\mu_{12}\mu_{21})}; \quad K_{22} = \frac{E_2 h}{(1-\mu_{12}\mu_{21})}; \\
K_{12} &= K_{21} = \frac{\mu_{12} E_2 h}{(1-\mu_{12}\mu_{21})}; \quad K_{66} = G_{12} h; \\
D_{11} &= \frac{E_1 h^3}{12(1-\mu_{12}\mu_{21})}; \quad D_{22} = \frac{E_2 h^3}{12(1-\mu_{12}\mu_{21})}; \\
D_{12} &= D_{21} = \frac{\mu_{12} E_2 h^3}{12(1-\mu_{12}\mu_{21})}; \quad D_{66} = \frac{G_{12} h^3}{12}.
\end{aligned}
$$

For a conical shell, the equilibrium equations are derived as [Naj *et al.*, 2008]:

$$
\begin{aligned}
&\sin\alpha \frac{\partial(xN_x)}{\partial x} + \frac{\partial N_{x\theta}}{\partial \theta} - \sin\alpha N_\theta = 0, \\
&\frac{\partial N_\theta}{\partial \theta} + \sin\alpha \frac{\partial(xN_{x\theta})}{\partial x} + \sin\alpha N_{x\theta} - \cos\alpha(N_{x\theta}\zeta_x + N_\theta \zeta_\theta) \\
&\qquad + \cos\alpha \left(\frac{\partial M_{x\theta}}{\partial x} + \frac{2}{x} M_{x\theta} + \frac{1}{x\sin\alpha} \frac{\partial M_\theta}{\partial \theta} \right) = 0, \\
&\sin\alpha \frac{\partial^2(xM_x)}{\partial x^2} + \frac{1}{x\sin\alpha} \frac{\partial^2 M_\theta}{\partial \theta^2} - \sin\alpha \frac{\partial M_\theta}{\partial x} + \frac{2}{x} \frac{\partial}{\partial x} \left(x \frac{\partial M_{x\theta}}{\partial \theta} \right) \\
&\qquad - \cos\alpha N_\theta - \left[\sin\alpha \frac{\partial(xN_x\zeta_x + xN_{x\theta}\zeta_\theta)}{\partial x} + \frac{\partial(N_{x\theta}\zeta_x + N_\theta\zeta_\theta)}{\partial \theta} \right] = 0,
\end{aligned} \tag{6}
$$

where

$$
\begin{aligned}
\zeta_x &= -\frac{\partial w}{\partial x}, \\
\zeta_\theta &= -\frac{1}{x\sin\alpha} \frac{\partial w}{\partial \theta} + \frac{v}{x\tan\alpha},
\end{aligned} \tag{7}
$$

where ζ_x and ζ_θ are the rotations of the normal to the middle surface about the x- and θ-axes, respectively.

For simplicity, the membrane solution of the equilibrium equations is considered [Meyers and Hyer, 1991]. For this aim, all the moment and rotations terms must be set equal to zero in the equilibrium equations. According to the symmetry of geometry and loading conditions, deflection in prebuckling configuration is assumed to be axisymmetric. By this assumption, the second relation of the equilibrium equations (6) vanishes. Considering the previously mentioned assumptions, the first and third relations of the equilibrium equations are simplified as [Torabi *et al.*, 2013]:

$$\begin{aligned} \frac{\partial(xN_{x0})}{\partial x} &= 0, \\ N_{\theta 0} &= 0, \end{aligned} \tag{8}$$

where the subscript 0 denotes the prebuckling state. The first of Eqs. (8) may be integrated which results in $N_{x0} = c_1/x$, where c_1 is the constant of integration. Substituting Eqs. (5) into Eqs. (8) and eliminating the terms containing derivatives of w_0 based on a membrane analysis, Eqs. (8) is obtained in terms of the displacement components as follows:

$$\begin{aligned} K_{11}\frac{\partial u_0}{\partial x} + K_{12}\left(\frac{u_0}{x} + \frac{w_0}{x\tan\alpha}\right) - N_x^C &= \frac{c_1}{x}, \\ K_{21}\frac{\partial u_0}{\partial x} + K_{22}\left(\frac{u_0}{x} + \frac{w_0}{x\tan\alpha}\right) - N_\theta^C &= 0. \end{aligned} \tag{9}$$

Solving Eqs. (9) and applying the in-plane boundary conditions ($u_0 = 0$ at $x = L_1, L$), the coefficient c_1 is obtained as

$$c_1 = \frac{(\mu_{12}N_\theta^C - N_x^C)(L - L_1)}{\ln(L) - \ln(L_1)}. \tag{10}$$

Finally, considering Eqs. (8) and (10) and assuming axisymmetric condition, the prebuckling force resultants induced by the absorption of moisture are obtained as:

$$\begin{aligned} N_{x0} = \frac{(\mu_{12}N_\theta^C - N_x^C)(L - L_1)}{x[\ln(L) - \ln(L_1)]} &= -\frac{E_1\beta_1 h\Delta C(L - L_1)}{x[\ln(L) - \ln(L_1)]}, \\ N_{\theta 0} &= 0, \\ N_{\theta 0} &= 0. \end{aligned} \tag{11}$$

The stability equations are obtained by consideration of the second variation of the functional of total potential energy as [Brush and Almroth, 1975; Torabi *et al.*, 2013]:

$$\begin{aligned} &\sin\alpha(xN_{x1})_{,x} + N_{x\theta 1,\theta} - \sin\alpha N_{\theta 1} = 0, \\ &N_{\theta 1,\theta} + \sin\alpha(xN_{x\theta 1})_{,x} + \sin\alpha N_{x\theta 1} - \cos\alpha(N_{x\theta 0}\zeta_{x1} + N_{\theta 0}\zeta_{\theta 1}) \\ &\quad + \cos\alpha\left(M_{x\theta 1,x} + \frac{2}{x}M_{x\theta 1} + \frac{M_{\theta 1,\theta}}{x\sin\alpha}\right) = 0, \end{aligned}$$

$$\sin\alpha(xM_{x1})_{,xx} + \frac{M_{\theta 1,\theta\theta}}{x\sin\alpha} - \sin\alpha M_{\theta 1,x} + \frac{2}{x}(xM_{x\theta 1,\theta})_{,x} - \cos\alpha N_{\theta 1} - [\sin\alpha(xN_{x0}\zeta_{x1} + xN_{x\theta 0}\zeta_{\theta 1})_{,x} + (N_{x\theta 0}\zeta_{x1} + N_{\theta 0}\zeta_{\theta 1})_{,\theta}] = 0. \tag{12}$$

The force resultants with subscript 0 present the prebuckling force resultants obtained from Eqs. (11).

For the state of stability, the force and moment resultants are:

$$\begin{aligned} N_{x1} &= K_{11}\varepsilon_{xm} + K_{12}\varepsilon_{\theta m}, \\ N_{\theta 1} &= K_{21}\varepsilon_{xm} + K_{22}\varepsilon_{\theta m}, \\ N_{x\theta 1} &= K_{66}\gamma_{x\theta m}, \\ M_{x1} &= D_{11}k_x + D_{12}k_\theta, \\ M_{\theta 1} &= D_{21}k_x + D_{22}k_\theta, \\ M_{x\theta 1} &= D_{66}k_{x\theta}. \end{aligned} \tag{13}$$

Substituting Eqs. (2), (11) and (13) into Eqs. (12), the stability equations in terms of the displacement components can be derived.

2.2. *Natural vibration of the orthotropic conical shell in a hygroscopic environment*

According to the Reissner–Naghdi thin shell theory [Leissa, 1993], considering the additional mass by absorbing moisture [Lyrintzis and Bofilios, 1990; Zhao *et al.*, 2013], we can establish a new motion equilibrium equation of the orthotropic conical shell including the pre-stresses effect as follows:

$$\begin{bmatrix} L_{11} & L_{12} & L_{13} \\ L_{21} & L_{22} & L_{23} \\ L_{31} & L_{32} & L_{33} \end{bmatrix} \begin{bmatrix} u \\ v \\ w \end{bmatrix} = \begin{bmatrix} F_x \\ F_\theta \\ F_z \end{bmatrix}, \tag{14}$$

where F_x, F_θ and F_z are the external forces loading the conical shell in x, θ and z directions, respectively. $L_{ij}(i,j = 1,2,3)$ are a coupled set of the differential operators and given as:

$$L_{11} = -K_{11}\frac{\partial^2}{\partial x^2} - \frac{K_{11}}{x}\frac{\partial}{\partial x} + \frac{K_{22}}{x^2} - \frac{K_{66}}{x^2\sin^2\alpha}\frac{\partial^2}{\partial\theta^2} + (1+\Delta C)\rho h\frac{\partial^2}{\partial t^2},$$

$$L_{12} = -\frac{(K_{12}+K_{66})}{x\sin\alpha}\frac{\partial^2}{\partial x\partial\theta} + \frac{(K_{22}+K_{66})}{x^2\sin\alpha}\frac{\partial}{\partial\theta},$$

$$L_{13} = -\frac{K_{12}}{x\tan\alpha}\frac{\partial}{\partial x} + \frac{K_{22}}{x^2\tan\alpha},$$

$$
\begin{aligned}
L_{21} &= -\frac{(K_{22}+K_{66})}{x^2\sin\alpha}\frac{\partial}{\partial\theta} - \frac{(K_{12}+K_{66})}{x\sin\alpha}\frac{\partial^2}{\partial x\partial\theta},\\
L_{22} &= -\left(\frac{K_{22}}{x^2\sin^2\alpha} + \frac{D_{22}}{x^4\sin^2\alpha\tan^2\alpha}\right)\frac{\partial^2}{\partial\theta^2} + \left(\frac{D_{66}}{x^3\tan\alpha} - \frac{K_{66}}{x}\right)\frac{\partial}{\partial x}\\
&\quad + \left(\frac{K_{66}}{x^2} + \frac{N_{\theta 0}}{x^2\tan^2\alpha}\right) - \left(K_{66} + \frac{D_{66}}{x^2\tan^2\alpha}\right)\frac{\partial^2}{\partial x^2} + (1+\Delta C)\rho h\frac{\partial^2}{\partial t^2},\\
L_{23} &= -\frac{(K_{22}-N_{\theta 0})}{x^2\sin\alpha\tan\alpha}\frac{\partial}{\partial\theta} - \frac{N_{x\theta 0}}{x\tan\alpha}\frac{\partial}{\partial x} + \frac{D_{22}}{x^3\sin\alpha\tan\alpha}\frac{\partial^2}{\partial x\partial\theta}\\
&\quad + \frac{(D_{12}+2D_{66})}{x^2\sin\alpha\tan\alpha}\frac{\partial^3}{\partial x^2\partial\theta} + \frac{D_{22}}{x^4\sin^3\alpha\tan\alpha}\frac{\partial^3}{\partial\theta^3},\\
L_{31} &= \frac{K_{22}}{x^2\tan\alpha} + \frac{K_{12}}{x\tan\alpha}\frac{\partial}{\partial x},\\
L_{32} &= \left(\frac{K_{22}}{x^2\sin\alpha\tan\alpha} - \frac{2D_{12}+2D_{22}+4D_{66}}{x^4\sin\alpha\tan\alpha}\right)\frac{\partial}{\partial\theta} + \frac{2D_{12}+D_{22}+4D_{66}}{x^3\sin\alpha\tan\alpha}\frac{\partial^2}{\partial x\partial\theta}\\
&\quad - \frac{D_{12}+4D_{66}}{x^2\sin\alpha\tan\alpha}\frac{\partial^3}{\partial x^2\partial\theta} - \frac{D_{22}}{x^4\sin^3\alpha\tan\alpha}\frac{\partial^3}{\partial\theta^3},\\
L_{33} &= \frac{K_{22}}{x^2\tan^2\alpha} + \left(\frac{D_{22}}{x^3} - \frac{N_{x0}}{x} - \frac{1}{x\sin\alpha}\frac{\partial N_{\theta 0}}{\partial\theta} - \frac{\partial N_{x0}}{\partial x}\right)\frac{\partial}{\partial x}\\
&\quad + \frac{2D_{11}}{x}\frac{\partial^3}{\partial x^3} + D_{11}\frac{\partial^4}{\partial x^4} - \frac{N_{x\theta 0}}{x\sin\alpha}\frac{\partial^2}{\partial x\partial\theta} + \frac{2D_{12}+4D_{66}}{x^2\sin^2\alpha}\frac{\partial^4}{\partial x^2\partial\theta^2}\\
&\quad - \left(\frac{1}{x\sin\alpha}\frac{\partial N_{x\theta 0}}{\partial x} + \frac{1}{x^2\sin^2\alpha}\frac{\partial N_{\theta 0}}{\partial\theta}\right)\frac{\partial}{\partial\theta} - \left(\frac{D_{22}}{x^2} + N_{x0}\right)\frac{\partial^2}{\partial x^2}\\
&\quad - \frac{2D_{12}+4D_{66}}{x^3\sin^2\alpha}\frac{\partial^3}{\partial x\partial\theta^2} + \frac{2D_{12}+2D_{22}+4D_{66}}{x^4\sin^2\alpha}\frac{\partial^2}{\partial\theta^2}\\
&\quad + \frac{D_{22}}{x^4\sin^4\alpha}\frac{\partial^4}{\partial\theta^4} + (1+\Delta C)\rho h\frac{\partial^2}{\partial t^2},
\end{aligned}
\tag{15}
$$

where ρ is the density of the material, ρh is the shell mass per unit area and $(1+\Delta C)$ accounts for the absorbed moisture. The force resultants N_{x0}, $N_{\theta 0}$ and $N_{x\theta 0}$ present the prebuckling force resultants induced by the hygroscopic environment.

Consider a conical shell with the immoveable simply supported boundary edges. The boundary conditions are assumed as:

$$
u = 0, \quad v = 0, \quad w = 0, \quad M_x = 0, \quad \text{at } x = L_1, L. \tag{16}
$$

The approximate solution for Eq. (14), satisfying the boundary conditions given by Eqs. (16), the displacements of the orthotropic conical shell in terms of wave

propagation can be written as [Laulagnet and Guyader, 1989; Naj *et al.*, 2008]:

$$\begin{aligned} u(x,\theta) &= \sum_{\varepsilon=0}^{1}\sum_{m=1}^{\infty}\sum_{n=0}^{\infty} U_{mn\varepsilon}\sin^2\left[k_m \ln\left(\frac{x}{L_1}\right)\right]\sin\left(n\theta+\frac{\varepsilon\pi}{2}\right), \\ v(x,\theta) &= \sum_{\varepsilon=0}^{1}\sum_{m=1}^{\infty}\sum_{n=0}^{\infty} V_{mn\varepsilon}\sin\left[k_m \ln\left(\frac{x}{L_1}\right)\right]\cos\left(n\theta+\frac{\varepsilon\pi}{2}\right), \\ w(x,\theta) &= \sum_{\varepsilon=0}^{1}\sum_{m=1}^{\infty}\sum_{n=0}^{\infty} W_{mn\varepsilon}x^{\frac{1-\mu_{12}}{2}}\sin\left[k_m \ln\left(\frac{x}{L_1}\right)\right]\sin\left(n\theta+\frac{\varepsilon\pi}{2}\right), \end{aligned} \tag{17}$$

where $k_m = [m\pi/\ln(L/L_1)]$ are the wavenumbers in the meridianal direction and its values are determined by the boundary condition. $\varepsilon = 0$ (respectively, 1) denotes antisymmetric (respectively, symmetric) modes. n is circumferential order, m is the meridianal order. To discuss conveniently, the orthotropic conical shell is just excited by the radial component of harmonic point driving force F_z, and for harmonic vibration, a time-dependent factor $e^{-j\omega t}$ will be suppressed throughout.

As described above, since the governing Eq. (14) is a set of partial differential equations with variable coefficients, it cannot be solved analytically. Instead, the present paper uses the Galerkin method to obtain an approximate solution. For governing Eq. (14), the weighted-integral statement of the Galerkin method can be expressed as follows:

$$\begin{aligned} \int_{L_1}^{L}(L_{11}u+L_{12}v+L_{13}w-F_x)\sin^2\left[k_m\ln\left(\frac{x}{L_1}\right)\right]\delta U_{mn\varepsilon}dx = 0, \\ \int_{L_1}^{L}(L_{21}u+L_{22}v+L_{23}w-F_\theta)\sin\left[k_m\ln\left(\frac{x}{L_1}\right)\right]\delta V_{mn\varepsilon}dx = 0, \\ \int_{L_1}^{L}(L_{31}u+L_{32}v+L_{33}w-F_z)x^{\frac{1-\mu_{12}}{2}}\sin\left[k_m\ln\left(\frac{x}{L_1}\right)\right]\delta W_{mn\varepsilon}dx = 0. \end{aligned} \tag{18}$$

The external forces F_x and F_θ are 0. Normal point exerts the conical shell with the amplitude of F_{zj}. Substituting Eqs. (17) into (18), one can obtain:

$$\left\{\begin{bmatrix} C_{11} & C_{12} & C_{13} \\ C_{21} & C_{22} & C_{23} \\ C_{31} & C_{32} & C_{33}+b\Delta C \end{bmatrix} + \omega^2\begin{bmatrix} R_{11} & 0 & 0 \\ 0 & R_{22} & 0 \\ 0 & 0 & R_{33} \end{bmatrix}\right\}\begin{bmatrix} U_{mn\varepsilon} \\ V_{mn\varepsilon} \\ W_{mn\varepsilon} \end{bmatrix} = \begin{bmatrix} 0 \\ 0 \\ \bar{F}_z \end{bmatrix}, \tag{19}$$

where $C_{ij}(i,j=1,2,3)$, R_{ii} and b are also similar coefficients expressed by the material elastic constants, geometric parameters and hygroscopic expansion coefficient, respectively and given in the appendix, ω is circular frequency, and $\bar{F}_z$ is given by:

$$\bar{F}_z = F_{zj}x_j^{\frac{1-\mu_{12}}{2}}\sin\left[k_m\ln\left(\frac{x_j}{L_1}\right)\right]\sin\left(n\theta_j+\frac{\varepsilon\pi}{2}\right)\Big/\varepsilon_n x_j\sin\alpha, \tag{20}$$

where ε_n is the Neumann factor. (x_j,θ_j) is the exciting point.

To derive the buckling moisture content for the conical shell, the determinant of the first coefficient matrix of Eq. (19) must be set equal to zero as:

$$\begin{vmatrix} C_{11} & C_{12} & C_{13} \\ C_{21} & C_{22} & C_{23} \\ C_{31} & C_{32} & C_{33} + b\Delta C \end{vmatrix} = 0. \tag{21}$$

Equation (21) may be written as:

$$\Delta C = \frac{\begin{array}{c} C_{13}C_{22}C_{31} + C_{11}C_{32}C_{23} + C_{12}C_{21}C_{33} - C_{12}C_{23}C_{31} \\ - C_{32}C_{21}C_{23} - C_{11}C_{22}C_{33} \end{array}}{b(C_{11}C_{22} - C_{12}C_{21})}. \tag{22}$$

As the variables m and n take a proper value respectively, the minimum value obtained from Eq. (22) is the critical buckling moisture content. The determinant of Eq. (19) can be solved by using linear algebra method for conical shell, and then the natural frequency is obtained [Soedel, 2004].

2.3. *The far field sound pressure in wave domain*

Moon and Spencer [1961] pointed out that the Helmholtz equation could be handled by separation of variables in 40 orthogonal curvilinear coordinates. The Helmholtz equation cannot be handled in the orthogonal curvilinear coordinates of the conical shell by use of separation of variables. Therefore, the conical shell will be divided into several cylinder parts. In the acoustic medium outside the shell, the sound pressure p_a satisfies the Helmholtz equation in the cylindrical coordinates [Cao *et al.*, 2011]:

$$\nabla^2 p + k_0^2 p = 0, \tag{23}$$

where the wavenumber k_0 is ω/c_a, c_a is the speed of sound in the air. Laplace operator ∇^2 is given by

$$\nabla^2 = \frac{1}{z^2}\frac{\partial^2}{\partial\theta^2} + \frac{1}{z}\frac{\partial}{\partial z}\left(z\frac{\partial}{\partial z}\right) + \frac{\partial^2}{\partial x^2}, \tag{24}$$

where x, θ and z denote the coordinate of meridianal, circumferential and radial directions in the circular cylindrical coordinate, respectively. The boundary condition at the jth part (approximate to cylindrical part) interface is

$$\left.\frac{\partial p_a}{\partial z}\right|_{z=r_j} = \omega^2\rho_0 w(x,\theta), \tag{25}$$

where ρ_0 is the density of the air and r_j is the radius of the jth cylinder. x is greater than L_j and less than L_{j+1}. In which, L_j and L_{j+1} are the localization coordinates of two ends for the jth cylinder in the x direction. These parameters are shown in Fig. 2.

Acoustic radiation from the conical shells is expressed by superposition of acoustic radiation from cylinder parts. Each cylinder is assumed to have infinite circular

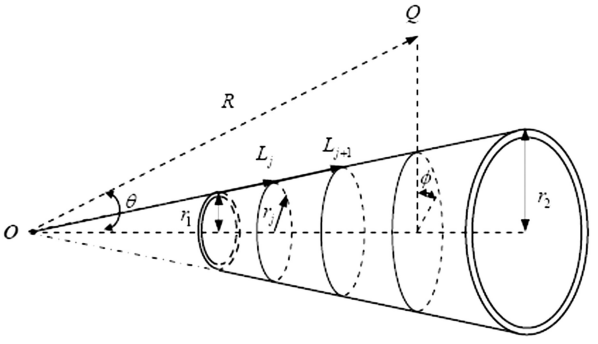

Fig. 2. Segments of conical shell.

cylindrical baffles at the two ends. The far field sound pressure will be derived in wavenumber domain. The Fourier transform is defined by

$$\tilde{f}(k) = \int_{-\infty}^{+\infty} f(x)e^{-ikx}dx. \tag{26}$$

The Fourier inverse transform is defined by

$$f(x) = \frac{1}{2\pi}\int_{-\infty}^{+\infty} \tilde{f}(k)e^{ikx}dk. \tag{27}$$

Taking the Fourier transform of Eq. (23) with respect to x, one obtains:

$$\left[\frac{1}{z^2}\frac{\partial^2}{\partial\theta^2} + \frac{1}{z}\frac{\partial}{\partial z}\left(z\frac{\partial}{\partial z}\right) + (k_0^2 - k^2)\right]\tilde{p}_{ja} = 0, \tag{28}$$

where p is replaced with $\tilde{p}_{ja}$ to denote the sound pressure induced by jth cylinder. $\tilde{p}_{ja}$ is the Fourier transform of p_{ja}. The far field sound pressure satisfies Sommerfeld radiation condition and the solution of Eq. (28) can be expressed by

$$\tilde{p}_{ja}(k,\theta,z) = \sum_{\varepsilon=0}^{1}\sum_{n=0}^{\infty} A_{n\varepsilon}H_n^{(1)}(\sqrt{k_0^2 - k^2}z)\sin\left(n\theta + \frac{\varepsilon\pi}{2}\right), \tag{29}$$

where $H_n^{(1)}(z)$ is the Hankel function of the first kind for order n. Taking the Fourier transform of Eq. (25) with respect to x, one obtain:

$$\sum_{\varepsilon=0}^{1}\sum_{n=0}^{\infty}\sqrt{k_0^2 - k^2}A_{n\varepsilon}H_n^{(1)'}(\sqrt{k_0^2 - k^2}r_j)\sin\left(n\theta + \frac{\varepsilon\pi}{2}\right) = \omega^2\rho_0\tilde{w}^j(k,\theta), \tag{30}$$

where $\tilde{w}^j(k,\theta)$ is the Fourier transform of $w^j(x,\theta)$. $w(x,\theta)$ is replaced with $w^j(x,\theta)$ to denote the surface radial displacement of the jth cylinder. Considering the third relation of Eq. (17), one obtains:

$$w^j(x,\theta) = \sum_{\varepsilon=0}^{1}\sum_{n}^{\infty} w_{n\varepsilon}^j(x)\sin\left(n\theta + \frac{\varepsilon\pi}{2}\right), \tag{31}$$

where $w^j_{n\varepsilon}(x)$ is defined by:

$$w^j_{n\varepsilon}(x) = \sum_m^{\infty} W_{mn\varepsilon} x^{\frac{1-\mu_{12}}{2}} \sin\left[k_m \ln\left(\frac{x}{L_1}\right)\right], \quad (L_j \le x \le L_{j+1}). \tag{32}$$

Therefore, $\tilde{w}^j(k,\theta)$ can be expressed by:

$$\tilde{w}^j(k,\theta) = \sum_{\varepsilon=0}^{1}\sum_n^{\infty} \tilde{w}^j_{n\varepsilon}(k)\sin\left(n\theta + \frac{\varepsilon\pi}{2}\right). \tag{33}$$

Combining Eq. (30) with (33), one obtains:

$$A_{n\varepsilon} = \frac{\omega^2\rho_0\tilde{w}^j_{n\varepsilon}(k)}{\sqrt{k_0^2-k^2}H_n^{(1)'}(\sqrt{k_0^2-k^2}r_j)}. \tag{34}$$

Substituting Eq. (34) into (29), and taking the Fourier inverse transform of Eq. (29), one obtains:

$$p_{ja}(x,\theta,z) = \frac{1}{2\pi}\int_{-\infty}^{+\infty}\sum_{\varepsilon=0}^{1}\sum_{n=0}^{\infty}\frac{\omega^2\rho_0\tilde{w}^j_{n\varepsilon}(k)H_n^{(1)}(\sqrt{k_0^2-k^2}z)}{\sqrt{k_0^2-k^2}H_n^{(1)'}(\sqrt{k_0^2-k^2}r_j)} \times \sin\left(n\theta+\frac{\varepsilon\pi}{2}\right)e^{ikx}dk. \tag{35}$$

By using large parameter approximation for $H_n^{(1)}(\sqrt{k_0^2-k^2}z)$ and stationary phase method [Junger and Feit, 1986], the far field sound pressure p_{ja} can be obtained in the spherical coordinates (stationary phase point $k = k_0\cos\theta$):

$$p_{ja}(R,\theta,\phi) = \frac{\omega^2\rho_0 e^{ik_0R}}{\pi k_0 R\sin\theta}\left[\sum_{\varepsilon=0}^{1}\sum_{n=0}^{\infty}\frac{\tilde{w}^j_{n\varepsilon}(k_0\cos\theta)}{H_n^{(1)'}(k_0r_j\sin\theta)}\sin\left(n\phi+\frac{\varepsilon\pi}{2}\right)(-i)^{n+1}\right], \tag{36}$$

where R is the distance from the origin to the far field point Q. ϕ is the azimuthal angle and θ is the polar angle. These parameters are illustrated in Fig. 2. Thus, the far field acoustic radiation $p_a(R,\theta,\varphi)$ from the conical shell is expressed by

$$p_a(R,\theta,\phi) = \frac{\omega^2\rho_0 e^{ik_0R}}{\pi k_0 R\sin\theta}\left[\sum_{j=1}^{s}\sum_{\varepsilon=0}^{1}\sum_{n=0}^{\infty}\frac{\tilde{w}^j_{n\varepsilon}(k_0\cos\theta)}{H_n^{(1)'}(k_0r_j\sin\theta)}\sin\left(n\phi+\frac{\varepsilon\pi}{2}\right)(-i)^{n+1}\right], \tag{37}$$

where s is the number of the segments for the conical shell. The far field sound pressure level (SPL) is calculated by

$$\mathrm{SPL} = 20\,\mathrm{Log10}\left(\frac{|p_a|}{p_0}\right), \tag{38}$$

where p_0 is the reference sound pressure 2.0×10^{-5} Pa.

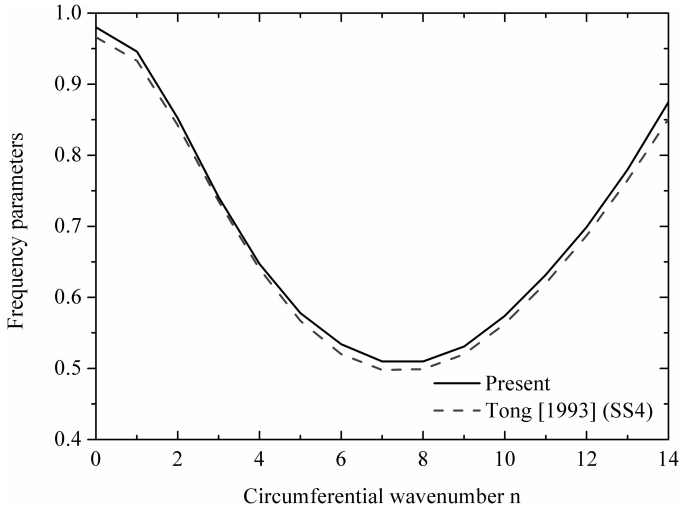

Fig. 3. Comparison of frequency parameters with Tong [1993], $m = 1$.

3. Validation

An immoveable simply supported isotropic conical shell with $\alpha = 30°$, $r_2 h = 100$, $\mu = 0.3, (L - L_1) \sin\alpha / r_2 = 0.25$ is considered for the validation of present work. The comparison of the present values for the frequency parameters defined as $\omega_c = \omega r_2 \sqrt{\rho h}/K_{11}$ with the data whose boundary condition is SS4 given by Tong [1993] is presented in Fig. 3. The meridianal wavenumber $m = 1$. As is expected, the comparison shows preferable well agreement. So it could be said that the vibration and acoustic radiation model of orthotropic conical shell presented in the paper is reliable and reasonable.

4. Results and Discussions

In this section, the vibration and acoustic response characteristics for the orthotropic conical shell excited by a harmonic concentrated force will be discussed by assuming that the conical shell is subjected to a uniform moisture content rise. First, the vibration and acoustic radiation characteristics for the orthotropic conical shell at incremental moisture content are researched. Second, to research the effects of different stiffness on the vibration and acoustic radiation characteristics for the orthotropic conical shell, the different ratios for circumferential Young's modulus to the meridianal will be assigned artificially. Finally, the effects of different semi-vertex angle on the vibration and acoustic responses of the conical shell are discussed.

An orthotropic composite conical shell is excited at $(x_j = (L + L_1)/2, \theta_j = 0)$ by harmonic excitation with amplitude of 1 N in normal direction is now considered

for a detailed investigation. Radii of the small end and large end are $r_1 = 0.75\,\text{m}$ and $r_2 = 1.0\,\text{m}$, respectively. L_1 is 1.5 m and L is 2.0 m. Thickness h of the cone is 0.004 m. Semi-vertex angle α of the cone is 30°. The mechanical properties for the carbon-epoxy composites are assumed to be as follows:

$$E_1 = 6.9\,\text{GPa}; \quad E_2 = 172.5\,\text{GPa}; \quad G_{12} = E_1/2\,\text{GPa};$$
$$\rho = 1600\,\text{kg/m}^3; \quad \mu_{21} = 0.25; \quad \beta_1 = 0.44; \quad \beta_2 = 0.0.$$

The density of the air and the velocity of the sound are assumed to be $\rho_0 = 1.21\,\text{kg/m}^3$ and $c_0 = 340\,\text{m/s}$.

4.1. *Free vibration study with incremental moisture contents*

All the hygroscopic load cases are designed below the critical buckling moisture content. According to Eq. (22), the critical buckling moisture content for this conical shell is $C_{\text{cr}} = 1.26\%$. The buckling mode has five meridianal and 11 circumferential waves. Therefore, six load cases are chosen with uniform moisture content rises ΔC of $0.63\%(0.5C_{\text{cr}})$, $0.95\%(0.75C_{\text{cr}})$, $1.13\%(0.9C_{\text{cr}})$, $1.20\%(0.95C_{\text{cr}})$, $1.23\%(0.975C_{\text{cr}})$ and $1.25\%(0.99C_{\text{cr}})$, respectively, and 0.0% is defined as the reference moisture content to represent the stress free state case.

The results obtained from the pre-stressed modal analysis are given in Table 1 which shows the lowest six natural frequencies for various values of moisture content rise and the modal indices are enclosed in parentheses. It is seen clearly that the natural frequency generally decreases with an increase in uniform moisture content. One can see from Table 1 that the meridianal and circumferential wavenumbers associated with the lowest frequency mode keep unchanged in lower moisture contents and reaches the modal indices corresponding to the lowest buckling mode near the critical buckling mode due to uniform moisture content rise. This is due to the reason that the stiffness of structure reduces with an increase in moisture content due to the compressive hygroscopic stresses.

As the natural frequencies associated with the orthotropic conical shell analyzed in the present work are close to each other, the natural frequencies in the excitation frequency range 0–1200 Hz are represented in terms of modal density (modes/Hz)

Table 1. Natural frequencies for immovable simply supported orthotropic conical shell with hygroscopic loads.

S. No.	Hygroscopic loads						
	$0C_{\text{cr}}$	$0.5C_{\text{cr}}$	$0.75C_{\text{cr}}$	$0.9C_{\text{cr}}$	$0.95C_{\text{cr}}$	$0.975C_{\text{cr}}$	$0.99C_{\text{cr}}$
1	223.9(1,7)	194.9(1,7)	178.6(1,7)	168.8(1,7)	163.3(4,11)	113.0(5,11)	58.7(5,11)
2	231.7(1,8)	203.7(1,8)	188.1(1,8)	178.7(1,8)	163.7(5,11)	133.1(4,11)	104.6(5,12)
3	232.9(1,6)	205.3(1,6)	189.9(1,6)	180.7(1,6)	164.8(1,7)	138.1(4,10)	108.4(4,11)
4	254.1(1,9)	228.6(1,9)	214.7(1,9)	206.4(1,9)	167.4(4,10)	142.4(5,12)	114.4(4,10)
5	261.0(1,5)	236.8(1,5)	223.6(1,5)	214.0(2,9)	175.0(1,8)	162.8(5,10)	131.1(5,10)
6	288.4(1,10)	266.0(1,10)	254.0(1,10)	215.8(1,5)	177.0(1,6)	163.1(1,7)	161.9(1,7)

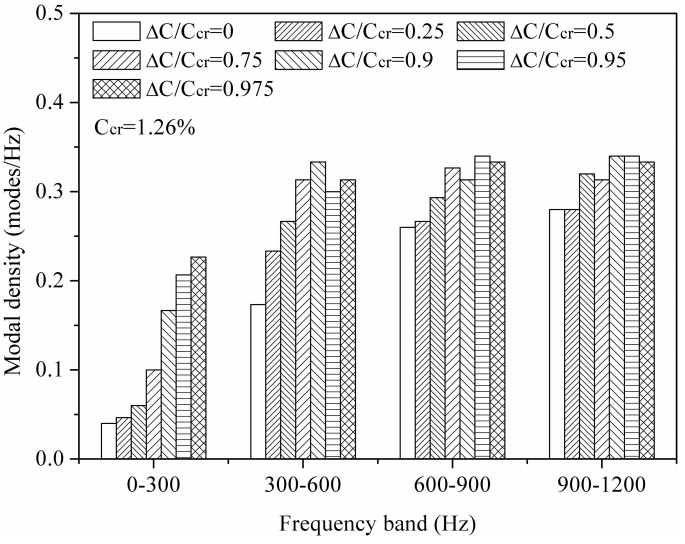

Fig. 4. Modal density variation with moisture content in constant frequency band.

in 300 Hz constant frequency bands. Modal density variation in 300 Hz frequency band is shown in Fig. 4. Shifting of natural frequencies toward lower frequency band can be clearly seen in 0–300 Hz band. It is the reason that the natural frequencies decrease with the moisture content which results in the number of modal increases in the lower frequency band.

4.2. *Acoustic response study with incremental moisture contents*

The sound field point for directivity patterns are defined in one circles with variation of azimuthal angle ϕ. The circle is defined by $R = \sqrt{((L_1+L)\cos\alpha)^2/4 + (50+(L_1+L)\sin\alpha/2)^2} = 50.92\,\text{m}$ and the polar angel $\theta = \tan^{-1}((100+(L_1+L)\sin\alpha)/((L_1+L)\cos\alpha)) = 88.3°$. The normal point force is located at $((L_1+L)/2, 0)$ with the amplitude of 1 N. The sampling point Q of sound field is located at $(50.92, 88.3°, 0°)$ in the spherical coordinates.

Figure 5 shows the effect of segments s for the conical shell and the wavenumbers m, n on the convergence of SPL. It is can be seen that the conical shell is divided into six parts and $m = 25$, $n = 25$ can yield good results for SPL in the frequency range. For large vertex cone, in order to obtain the convergent sound pressure, the value of s should be a little larger.

The SPL of the orthotropic conical shell with $0.0\%(0C_{\text{cr}})$, $0.63\%(0.5C_{\text{cr}})$ and $1.23\%(0.975C_{\text{cr}})$ moisture contents are plotted in Fig. 6. It can be seen that the effect of uniform incremental moisture contents on the SPL is obvious. The SPL floats to the low frequency direction due to the reduction of natural frequencies, which is more significant in lower frequency.

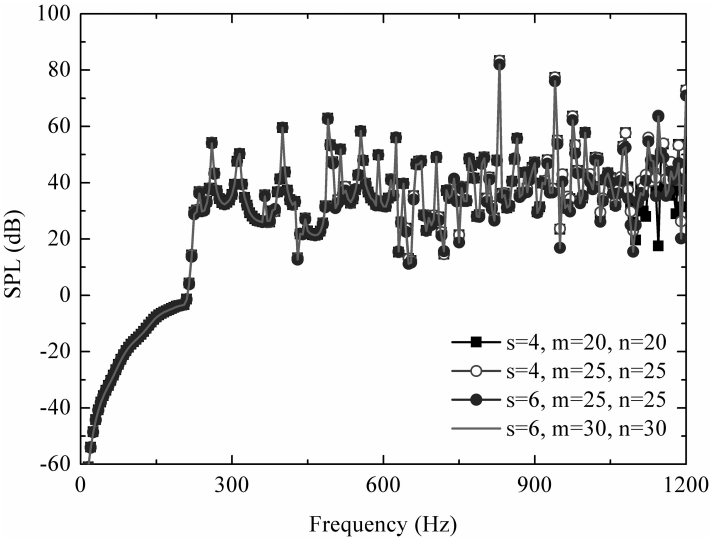

Fig. 5. SPL convergence of orthotropic conical shell.

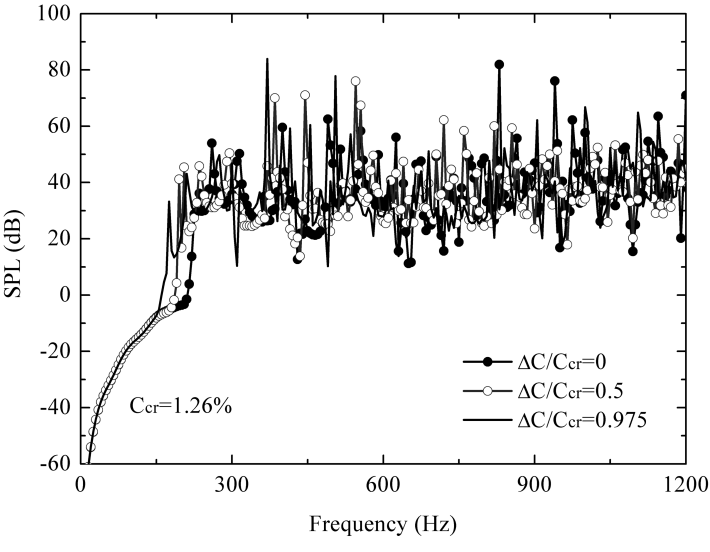

Fig. 6. SPL for various moisture contents.

For further investigation of overall SPL is calculated for different moisture contents in the entire frequency band as shown in Fig. 7. From Fig. 7 one can see the overall SPL generally decreases with the moisture content. When the moisture content $\Delta C/C_{\rm cr} = 0.975$, which is closer to the critical buckling moisture content, there is a marginal increment in the overall SPL.

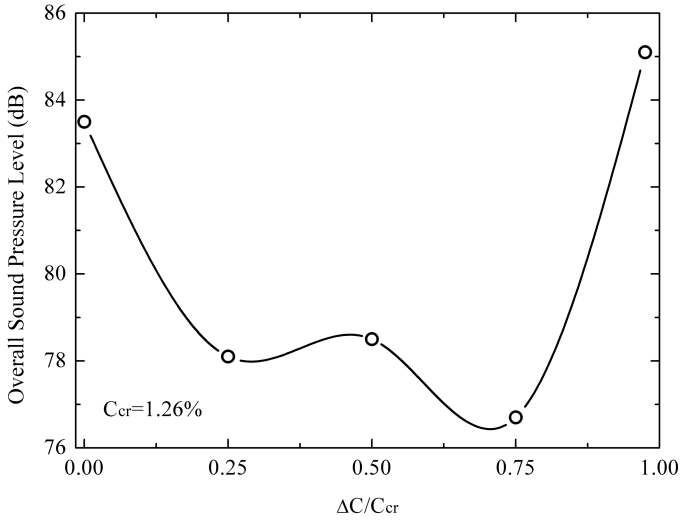

Fig. 7. Overall SPL for various moisture contents.

4.3. *Effects of different stiffness on the acoustic response of the orthotropic conical shell*

In this section, to research the effects of different stiffness on the acoustic responses of the orthotropic conical shell, we keep the circumferential Young's modulus E_2 unchanged in 172.5 GPa while assign meridianal Young's modulus E_1 artificially increase from 6.9 to 34.5 and 172.5 GPa, so that the stiffness of the orthotropic conical shell increase gradually as the ratio of E_2 to E_1 reduces from 25 to 5 and 1. When the ratio reduces to one, the orthotropic conical shell is equivalent to an isotropic conical shell approximately.

The effects of the different stiffness on the modal density of the orthotropic conical shell are shown in Fig. 8. It indicates that the modal density decreases with the increasing stiffness of the conical shell in the whole frequency band.

SPL for various stiffnesses is shown in Fig. 9. It can be seen clearly in Fig. 9 that the SPL decreases with the decrease of the ratio of E_2 to E_1 in the lower frequency range. For the increases of the stiffness of the conical shell with the decrease of the ratio of modulus, the fundamental frequency of the conical shells increases with the ratio of 25, 5 and 1, and the first peaks of the curves move to high frequency direction due to the increase of fundamental natural frequency.

To obtain a clear picture, the overall SPL for the entire frequency band is computed for different stiffnesses and the results are shown in Fig. 10. It can be seen that the overall SPL decreases in fluctuation with the reduction of the ratio of E_2/E_1 generally.

A further study for the orthotropic properties of the conical shell on the acoustic radiation characteristics is presented in Fig. 11, which includes two plots: one is

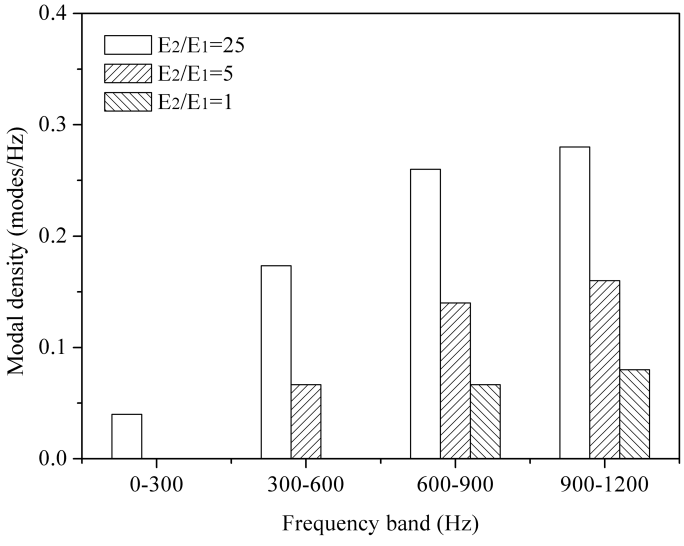

Fig. 8. Modal density variation with stiffness in constant frequency band.

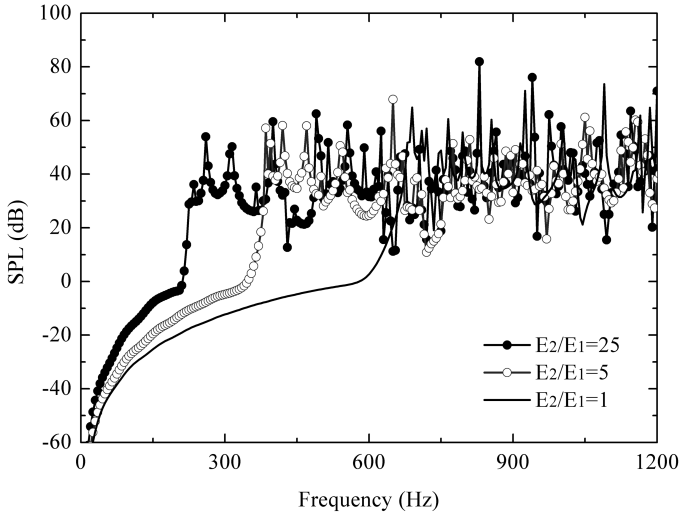

Fig. 9. SPL for various stiffnesses.

orthotropic conical shell, and the other one is isotropic conical shell which has the same first modal frequency (fundamental frequency) as the orthotropic conical shell. Then the SPLs can be compared at different frequencies. The ratio of circumferential Young's modulus to the meridianal of the orthotropic conical shell equals 5. It is can be seen in Fig. 11 that both of the two plots have the resonant amplitude of SPL at fundamental frequency 385.2 Hz. The two plots are almost the same SPL

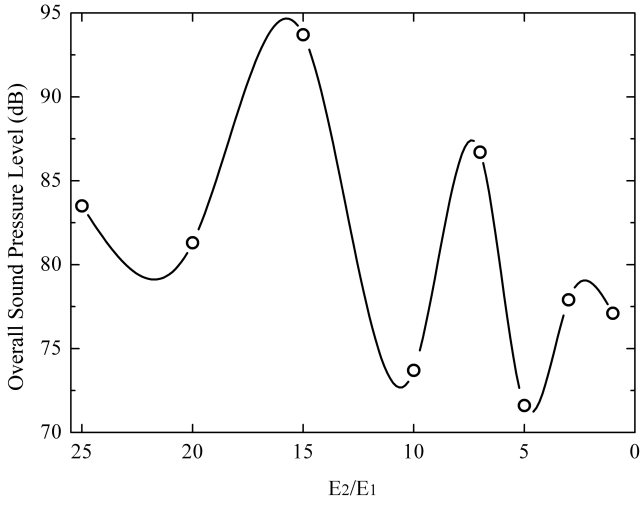

Fig. 10. Overall SPL for various stiffnesses.

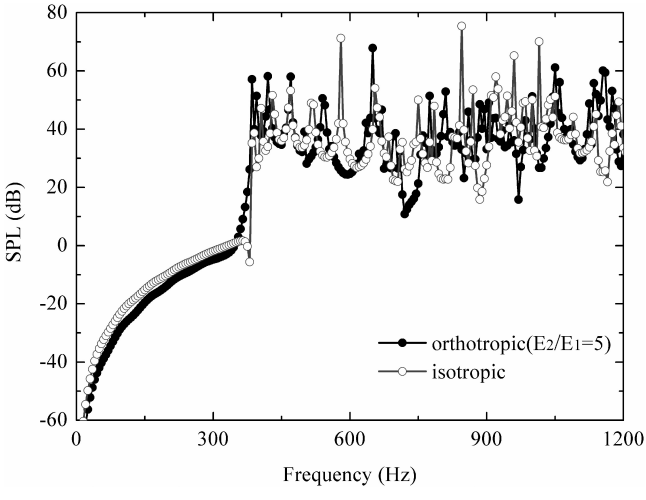

Fig. 11. Comparison of SPL for the orthotropic conical shell with the isotropic both has the same fundamental frequency.

amplitude in the frequency band less than the fundamental frequency, but show great different after the fundamental frequency.

4.4. *Effects of different semi-vertex angle on the acoustic responses of the orthotropic conical shell*

As the sketch shown in Fig. 12, to research the effects of different semi-vertex angle on the acoustic responses of the orthotropic conical shell, we keep the height of

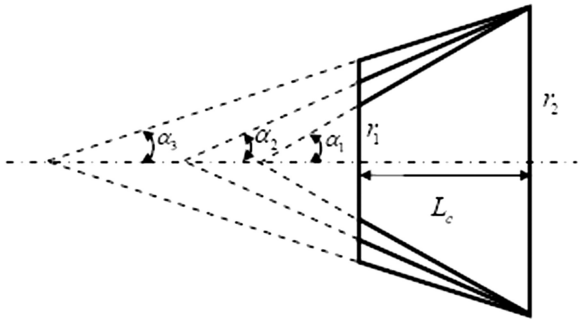

Fig. 12. The sketch of different semi-vertex angle of the conical shell.

the conical shell $L_C = 0.5\,\text{m}$, the thickness $h = 0.004\,\text{m}$ and the radius of large end $r_2 = 1.0\,\text{m}$ of the conical shell unchanged while assign the semi-vertex angle artificially decrease from 60° to 10° and 1°. The material properties are same as those given in the beginning of Sec. 4. When the semi-vertex angle reduces to 1°, the orthotropic conical shell is equivalent to an orthotropic cylindrical shell approximately.

The modal density of the orthotropic conical shell variation with the semi-vertex angle is shown in Fig. 13. It indicates that the modal density increases with the decreasing semi-vertex angle of the conical shell in constant frequency band.

The SPL and overall SPL for the orthotropic conical shell with various semi-vertex angles are shown in Figs. 14 and 15. It can be seen clearly that the SPL and

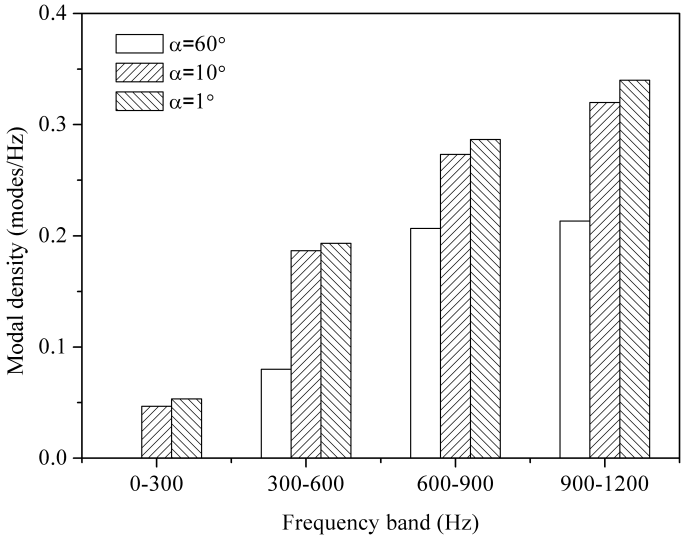

Fig. 13. Modal density variation with semi-vertex angle in constant frequency band.

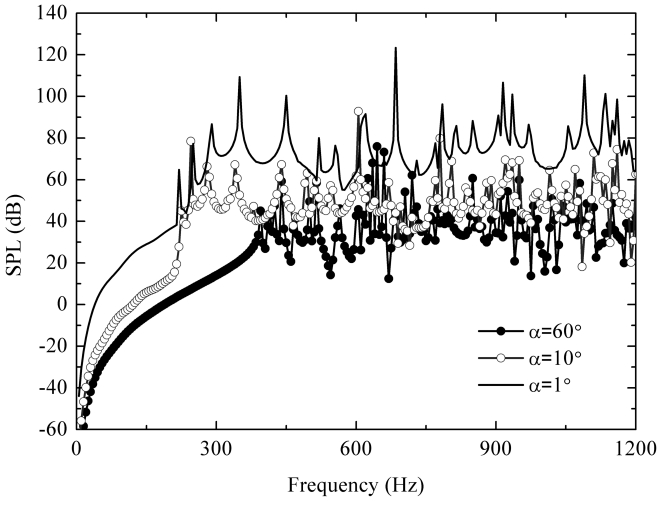

Fig. 14. SPL for various semi-vertex angles.

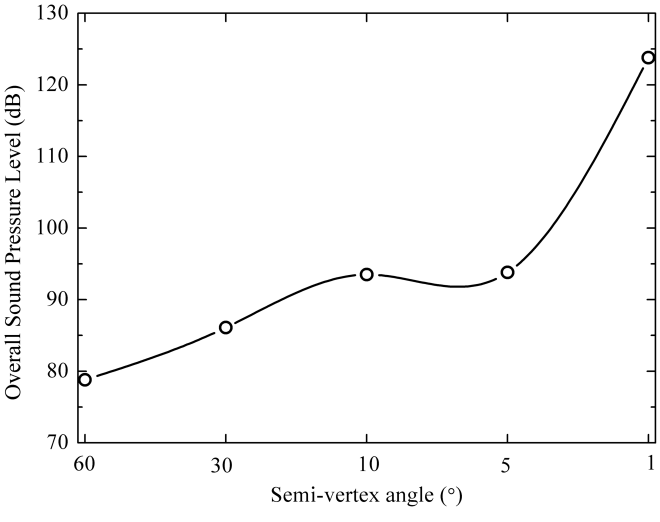

Fig. 15. Overall SPL for various semi-vertex angles.

overall SPL generally increases with the decrease of the semi-vertex angle in the whole frequency range. The numbers of the resonant amplitude increase with the decrease of the semi-vertex angle due to the increment of the modal density.

5. Conclusions

Analytical study considering the hygroscopic effect on the vibration and acoustic radiation of an orthotropic composite conical shell excited by a harmonic

concentrated force is carried out in present paper. Theoretical solution considering the effects of hygroscopic stress and mass addition caused by moisture absorption is obtained. First, to verify the theoretical model, natural frequencies parameters are validated through the results available in the literature for the isotropic conical shell. The comparisons indicate that the theoretical model of the orthotropic conical shell in present work is reliable and reasonable. Second, with the critical buckling moisture content as a parameter, the natural frequencies and far field sound pressure with incremental moisture content are computed respectively with the immovable simply supported boundary condition. Furthermore, the decreasing ratios of circumferential Young's modulus to the meridianal are set artificially to study the effect of different stiffnesses on the acoustic radiation characteristics of the orthotropic conical shell. Finally, the effects of different semi-vertex angle on the acoustic responses of the orthotropic conical shell are studied.

From the free vibration studies, it is found that the natural frequencies decrease with the increase of the moisture content. The meridianal and circumferential wavenumbers associated with the lowest frequency mode reaches the modal indices corresponding to the lowest buckling mode near the critical buckling moisture content due to uniform moisture content rise. The shifting of natural frequencies toward lower frequency band can be clearly seen in lower frequency band. The SPL floats to the low frequency direction with the increase of moisture content due to the reduction of natural frequency. There is a marginal increase in overall SPL near the critical buckling moisture content. For the increases of the stiffness of the conical shell with the decrease of the ratio of the circumferential modulus to the meridianal, the SPL decreases with the decrease of the ratio in the low frequency range, and the first peaks of the curves move to the higher frequency direction due to the increase of fundamental natural frequency. In the comparative study for the SPL of the orthotropic conical shell with the isotropic both has the same fundamental frequency, the two SPL plots are almost the same amplitude in the frequency band less than the fundamental frequency, but show great different after the fundamental frequency. SPL increases with the decrease of the semi-vertex angle in the whole frequency range.

Acknowledgment

This work is supported by the National Natural Science Foundation of China (Grant Nos. 11321062 and 11472206).

Appendix

$$C_{11} = \int_{L_1}^{L} \left\{ -\frac{2k_m^2 K_{11}}{x^2} \cos\left[2k_m \ln\left(\frac{x}{L_1}\right)\right] \sin^2\left[k_m \ln\left(\frac{x}{L_1}\right)\right] + \frac{K_{22}}{x^2} \sin^4\left[k_m \ln\left(\frac{x}{L_1}\right)\right] + \frac{n^2 K_{66}}{x^2 \sin^2\alpha} \sin^4\left[k_m \ln\left(\frac{x}{L_1}\right)\right] \right\} dx, \tag{A.1}$$

$$C_{12} = \int_{L_1}^{L} \left\{ -\frac{n(K_{22}+K_{66})}{x^2 \sin\alpha} \sin^3\left[k_m \ln\left(\frac{x}{L_1}\right)\right] + \frac{nk_m(K_{12}+K_{66})}{x^2 \sin\alpha} \cos\left[k_m \ln\left(\frac{x}{L_1}\right)\right] \sin^2\left[k_m \ln\left(\frac{x}{L_1}\right)\right] \right\} dx, \tag{A.2}$$

$$C_{13} = \int_{L_1}^{L} \left\{ -\frac{K_{12}}{x^{(3+\mu_{12})/2} \tan\alpha} \left\{ \left(\frac{1-\mu_{12}}{2}\right) \sin^3\left[k_m \ln\left(\frac{x}{L_1}\right)\right] + k_m \cos\left[k_m \ln\left(\frac{x}{L_1}\right)\right] \sin^2\left[k_m \ln\left(\frac{x}{L_1}\right)\right] \right\} + \frac{K_{22}}{x^{(3+\mu_{12})/2} \tan\alpha} \sin^3\left[k_m \ln\left(\frac{x}{L_1}\right)\right] \right\} dx, \tag{A.3}$$

$$C_{21} = \int_{L_1}^{L} \left\{ -\frac{n(K_{22}+K_{66})}{x^2 \sin\alpha} \sin^3\left[k_m \ln\left(\frac{x}{L_1}\right)\right] - \frac{(K_{12}+K_{66})nk_m}{x^2 \sin\alpha} \sin\left[k_m \ln\left(\frac{x}{L_1}\right)\right] \sin\left[2k_m \ln\left(\frac{x}{L_1}\right)\right] \right\} dx, \tag{A.4}$$

$$C_{22} = \int_{L_1}^{L} \left\{ n^2 \left(\frac{K_{22}}{x^2 \sin^2\alpha} + \frac{D_{22}}{x^4 \sin^2\alpha \tan^2\alpha}\right) \sin^2\left[k_m \ln\left(\frac{x}{L_1}\right)\right] + k_m \left(\frac{D_{66}}{x^4 \tan^2\alpha} - \frac{K_{66}}{x^2}\right) \cos\left[k_m \ln\left(\frac{x}{L_1}\right)\right] \sin\left[k_m \ln\left(\frac{x}{L_1}\right)\right] + \frac{K_{66}}{x^2} \sin^2\left[k_m \ln\left(\frac{x}{L_1}\right)\right] + k_m \left(\frac{K_{66}}{x^2} + \frac{D_{66}}{x^4 \tan^2\alpha}\right) \cos\left[k_m \ln\left(\frac{x}{L_1}\right)\right] \sin\left[k_m \ln\left(\frac{x}{L_1}\right)\right] + k_m^2 \left(\frac{K_{66}}{x^2} + \frac{D_{66}}{x^4 \tan^2\alpha}\right) \sin^2\left[k_m \ln\left(\frac{x}{L_1}\right)\right] \right\} dx, \tag{A.5}$$

$$C_{23} = \int_{L_1}^{L} \left\{ -\frac{nK_{22}}{x^{(3+\mu_{12})/2} \sin\alpha \tan\alpha} \sin^2\left[k_m \ln\left(\frac{x}{L_1}\right)\right] + \frac{nD_{22}}{x^{(7+\mu_{12})/2} \sin\alpha \tan\alpha} \left(\frac{1-\mu_{12}}{2}\right) \sin^2\left[k_m \ln\left(\frac{x}{L_1}\right)\right] + \frac{nk_m D_{22}}{x^{(7+\mu_{12})/2} \sin\alpha \tan\alpha} \cos\left[k_m \ln\left(\frac{x}{L_1}\right)\right] \sin\left[k_m \ln\left(\frac{x}{L_1}\right)\right] - \frac{n(D_{12}+2D_{66})}{x^{(7+\mu_{12})/2} \sin\alpha \tan\alpha} \mu_{12} k_m \cos\left[k_m \ln\left(\frac{x}{L_1}\right)\right] \sin\left[k_m \ln\left(\frac{x}{L_1}\right)\right] \right.$$

$$- \frac{n(D_{12}+2D_{66})}{x^{(7+\mu_{12})/2}\sin\alpha\tan\alpha}\left(\frac{1-\mu_{12}^2}{4}+k_m^2\right)\sin^2\left[k_m\ln\left(\frac{x}{L_1}\right)\right]$$

$$- \frac{n^3 D_{22}}{x^{(7+\mu_{12})/2}\sin^3\alpha\tan\alpha}\sin^2\left[k_m\ln\left(\frac{x}{L_1}\right)\right]\Bigg\}dx, \tag{A.6}$$

$$C_{31} = \int_{L_1}^{L}\Bigg\{\left(\frac{K_{12}k_m}{x^{(3+\mu_{12})/2}\tan\alpha}\right)\sin\left[2k_m\ln\left(\frac{x}{L_1}\right)\right]\sin\left[k_m\ln\left(\frac{x}{L_1}\right)\right]$$

$$+ \frac{K_{22}}{x^{(3+\mu_{12})/2}\tan\alpha}\sin^3\left[k_m\ln\left(\frac{x}{L_1}\right)\right]\Bigg\}dx, \tag{A.7}$$

$$C_{32} = \int_{L_1}^{L}\Bigg\{-\frac{nK_{22}}{x^{(3+\mu_{12})/2}\sin\alpha\tan\alpha}\sin^2\left[k_m\ln\left(\frac{x}{L_1}\right)\right]$$

$$+ \frac{n(2D_{12}+2D_{22}+4D_{66})}{x^{(3+\mu_{12})/2}\sin\alpha\tan\alpha}\sin^2\left[k_m\ln\left(\frac{x}{L_1}\right)\right]$$

$$- \frac{nk_m(2D_{12}+D_{22}+4D_{66})}{x^{(7+\mu_{12})/2}\sin\alpha\tan\alpha}\cos\left[k_m\ln\left(\frac{x}{L_1}\right)\right]\sin\left[k_m\ln\left(\frac{x}{L_1}\right)\right]$$

$$- \frac{nk_m^2(D_{12}+4D_{66})}{x^{(7+\mu_{12})/2}\sin\alpha\tan\alpha}\sin^2\left[k_m\ln\left(\frac{x}{L_1}\right)\right]$$

$$- \frac{nk_m(D_{12}+4D_{66})}{x^{(7+\mu_{12})/2}\sin\alpha\tan\alpha}\cos\left[k_m\ln\left(\frac{x}{L_1}\right)\right]\sin\left[k_m\ln\left(\frac{x}{L_1}\right)\right]$$

$$- \frac{D_{22}n^3}{x^{(7+\mu_{12})/2}\sin^3\alpha\tan\alpha}\sin^2\left[k_m\ln\left(\frac{x}{L_1}\right)\right]\Bigg\}dx, \tag{A.8}$$

$$C_{33} = \int_{L_1}^{L}\Bigg\{\frac{K_{22}}{x^{1+\mu_{12}}\tan^2\alpha}\sin^2\left[k_m\ln\left(\frac{x}{L_1}\right)\right]$$

$$+ \frac{D_{22}}{x^{3+\mu_{12}}}\left(\frac{1-\mu_{12}}{2}\right)\sin^2\left[k_m\ln\left(\frac{x}{L_1}\right)\right]$$

$$+ \frac{k_m D_{22}}{x^{3+\mu_{12}}}\cos\left[k_m\ln\left(\frac{x}{L_1}\right)\right]\sin\left[k_m\ln\left(\frac{x}{L_1}\right)\right]$$

$$+ \frac{\mu_{12}k_m D_{22}}{x^{3+\mu_{12}}}\cos\left[k_m\ln\left(\frac{x}{L_1}\right)\right]\sin\left[k_m\ln\left(\frac{x}{L_1}\right)\right]$$

$$+ \frac{D_{22}}{x^{3+\mu_{12}}}\left(\frac{1-\mu_{12}^2}{4}+k_m^2\right)\sin^2\left[k_m\ln\left(\frac{x}{L_1}\right)\right]$$

$$+ \frac{2D_{11}}{x^{3+\mu_{12}}}\left[\frac{(3\mu_{12}^2+6\mu_{12}-1)k_m}{4}-k_m^3\right]\cos\left[k_m\ln\left(\frac{x}{L_1}\right)\right]\sin\left[k_m\ln\left(\frac{x}{L_1}\right)\right]$$

$$+\frac{2D_{11}}{x^{3+\mu_{12}}}\left[\frac{(3+3\mu_{12})k_m^2}{2}-\frac{\mu_{12}^3+3\mu_{12}^2-\mu_{12}-3}{8}\right]\sin^2\left[k_m\ln\left(\frac{x}{L_1}\right)\right]$$

$$+\frac{D_{11}}{x^{3+\mu_{12}}}\left[(4+2\mu_{12})k_m^3-\frac{(\mu_{12}^3+6\mu_{12}^2+7\mu_{12}-2)k_m}{2}\right]$$

$$\cdot\cos\left[k_m\ln\left(\frac{x}{L_1}\right)\right]\sin\left[k_m\ln\left(\frac{x}{L_1}\right)\right]$$

$$+\frac{D_{11}}{x^{3+\mu_{12}}}\left[k_m^4-\frac{3\mu_{12}^2+12\mu_{12}+7}{2}k_m^2+\frac{\mu_{12}^4+8\mu_{12}^3+14\mu_{12}^2-8\mu_{12}-15}{16}\right]$$

$$\cdot\sin^2\left[k_m\ln\left(\frac{x}{L_1}\right)\right]$$

$$+\frac{n^2(2D_{12}+4D_{66})}{x^{3+\mu_{12}}\sin^2\alpha}\left(\frac{1-\mu_{12}}{2}\right)\sin^2\left[k_m\ln\left(\frac{x}{L_1}\right)\right]$$

$$+\frac{n^2k_m(2D_{12}+4D_{66})}{x^{3+\mu_{12}}\sin^2\alpha}\cos\left[k_m\ln\left(\frac{x}{L_1}\right)\right]\sin\left[k_m\ln\left(\frac{x}{L_1}\right)\right]$$

$$+\frac{n^2\mu_{12}k_m(2D_{12}+4D_{66})}{x^{3+\mu_{12}}\sin^2\alpha}\cos\left[k_m\ln\left(\frac{x}{L_1}\right)\right]\sin\left[k_m\ln\left(\frac{x}{L_1}\right)\right]$$

$$+\frac{n^2(2D_{12}+4D_{66})}{x^{3+\mu_{12}}\sin^2\alpha}\left(\frac{1-\mu_{12}^2}{4}+k_m^2\right)\sin^2\left[k_m\ln\left(\frac{x}{L_1}\right)\right]$$

$$-\frac{(2D_{12}+2D_{22}+4D_{66})n^2}{x^{3+\mu_{12}}\sin^2\alpha}\sin^2\left[k_m\ln\left(\frac{x}{L_1}\right)\right]$$

$$+\frac{D_{22}n^4}{x^{3+\mu_{12}}\sin^4\alpha}\sin^2\left[k_m\ln\left(\frac{x}{L_1}\right)\right], \tag{A.9}$$

$$R_{11}=-\int_{L_1}^{L}(1+\Delta C)\rho h\sin^4\left[k_m\ln\left(\frac{x}{L_1}\right)\right]dx, \tag{A.10}$$

$$R_{22}=-\int_{L_1}^{L}(1+\Delta C)\rho h\sin^2\left[k_m\ln\left(\frac{x}{L_1}\right)\right]dx, \tag{A.11}$$

$$R_{33}=-\int_{L_1}^{L}(1+\Delta C)\rho h x^{1-\mu_{12}}\sin^2\left[k_m\ln\left(\frac{x}{L_1}\right)\right]dx, \tag{A.12}$$

$$b=-\frac{E_1\beta_1 h(L-L_1)}{\ln(L)-\ln(L_1)}\int_{L_1}^{L}\left\{\frac{\mu_{12}k_m}{x^{2+\mu_{12}}}\cos\left[k_m\ln\left(\frac{x}{L_1}\right)\right]\sin\left[k_m\ln\left(\frac{x}{L_1}\right)\right]\right.$$

$$\left.+\frac{1}{x^{2+\mu_{12}}}\left(\frac{1-\mu_{12}^2}{4}+k_m^2\right)\sin^2\left[k_m\ln\left(\frac{x}{L_1}\right)\right]\right\}dx. \tag{A.13}$$

References

Brush, D. O. and Almroth, B. O. [1975] *Buckling of Bars, Plates and Shells* (McGraw-Hill, New York), pp. 190–217.

Cao, X., Hua, H. and Chen, Y. [2011] "Acoustic radiation from laminated conical shells," *Journal of Ship Mechanics* **15**(12), 1439–1450.

Cao, X., Hua, H. and Ma, C. [2012] "Acoustic radiation from shear deformable stiffened laminated cylindrical shells," *Journal of Sound and Vibration* **331**, 651–670.

Caresta, M. and Kessissoglou, N. J. [2008] "Vibration of fluid loaded conical shells," *Journal of the Acoustical Society of America* **124**(4), 2068–2077.

Gan, L., Li, X. and Zhang, Z. [2009] "Free vibration analysis of ring-stiffened cylindrical shells using wave propagation approach," *Journal of Sound and Vibration* **326**(3), 633–646.

Geng, Q. and Li, Y. [2012] "Analysis of dynamic and acoustic radiation characters for a flat plate under thermal environments," *International Journal of Applied Mechanics* **4**, 1250028.

Gonella, S., Greene, M. S. and Kam Liu, W. [2011] "Characterization of heterogeneous solids via wave methods in computational microelasticity," *Journal of the Mechanics and Physics of Solids* **59**, 959–974.

Hui, T. and Oskay, C. [2014] "A high order homogenization model for transient dynamics of heterogeneous media including micro-inertia effects," *Computer Methods in Applied Mechanics and Engineering* **273**, 181–203.

Jeyaraj, P., Padmanabhan, C. and Ganesan, N. [2011] "Vibro-acoustic response of a circular isotropic cylindrical shell under a thermal environment," *International Journal of Applied Mechanics* **3**(3), 525–541.

Junger, M. C. and Feit, D. [1986] *Sound, Structures, and Their Interactions*, 2nd edn. (MIT Press, Cambridge), pp. 151–231.

Kafesaki, M., Sigalas, M. M. and Economou, E. N. [1995] "Elastic wave band gaps in 3-d periodic polymer matrix composites," *Solid State Communications* **96**(5), 285–289.

Kaw, A. K. [2006] *Mechanics of Composite Materials*, 2nd edn. (Taylor and Francis, Boca Raton), pp. 160–167.

Lam, K. Y. and Li, H. [1999a] "On free vibration of a rotating truncated circular orthotropic conical shell," *Composites: Part B* **30**, 135–144.

Lam, K. Y. and Hua, L. [1999b] "Influence of boundary conditions on the frequency characteristics of a rotating truncated circular conical shell," *Journal of Sound and Vibration* **223**(2), 171–195.

Laulagnet, B. and Guyader, J. L. [1989] "Modal analysis of a shell's acoustic radiation in light and heavy fluids," *Journal of Sound and Vibration* **131**(3), 397–415.

Leissa, A. W. [1993] *Vibration of Shells* (Ohio, U.S: Acoustical Society of America), pp. 331–397

Luo, W. and Schmidt, H. [2009] "Three-dimensional propagation and scattering around a conical seamount," *Journal of the Acoustical Society of America* **125**(1), 52–65.

Lyrintzis, C. S. and Bofilios, D. A. [1990] "Hygrothermal effects on structure-borne noise transmission of stiffened laminated composite plates," *Journal of Aircraft* **27**(8), 722–730.

Meyers, C. A. and Hyer, M. W. [1991] "Thermal buckling and postbuckling of symmetrically laminated composite plates," *Journal of Thermal Stresses* **14**, 519–540.

Moon, P. and Spencer, D. E. [1961] *Field Theory Handbook*, 2nd edn. (Spriger-Verlag, Berlin), pp. 136–216.

Naj, R., Sabzikar Boroujerdy, M. and Eslami, M. R. [2008] "Thermal and mechanical instability of functionally graded truncated conical shells," *Thin-Walled Structures* **46**, 65–78.

Parhi, P. K., Bhattacharyya, S. K. and Sinha, P. K. [2001] "Hygrothermal effects on the dynamic behavior of multiple delaminated composite plates and shells," *Journal of Sound and Vibration* **248**(2), 195–214.

Shen, H. [2001] "The effects of hygrothermal conditions on the postbuckling of shear deformable laminated cylindrical shells," *International Journal of Solid and Structures* **38**, 6357–6380.

Soedel, W. [2004] *Vibrations of Shells and Plates*, 3rd edn. (Marcel Dekker, New York), pp. 75–144.

Suzuki, T. and Yu, P. K. L. [1998] "Complex elastic wave band structures in three-dimensional periodic elastic media," *Journal of the Mechanics and Physics of Solids* **46**(1), 115–138.

Tong, L. Y. [1993] "Free vibration of orthotropic conical shells," *International Journal of Engineering Science* **31**(5), 719–733.

Torabi, J., Kiani, Y. and Eslami, M. R. [2013] "Linear thermal buckling analysis of truncated hybrid FGM conical shells," *Composites: Part B* **50**, 265–272.

Whitney, J. M. and Ashton, J. E. [1971] "Effect of environment on the elastic response of layered composite plates," *American Institute of Aeronautics and Astronautics Journal* **9**(9), 1708–1713.

Zhang, X. M. [2002] "Frequency sanalysis of submerged cylindrical shells with the wave propagation approach," *International Journal of Mechanical Sciences* **44**(7), 1259–1273.

Zhang, X. M., Liu, G. R. and Lam, K. Y. [2001] "Coupled vibration analysis of fluid-filled cylindrical shells using the wave propagation approach," *Applied Acoustics* **62**(3), 229–243.

Zhao, X., Geng, Q. and Li, Y. [2013] "Vibration and acoustic response of an orthotropic composite laminated plate in a hygroscopic environment," *Journal of the Acoustical Society of America* **133**(3), 1433–1442.